HHS Public Access

Author manuscript

J Phys Chem B. Author manuscript; available in PMC 2023 July 09.

Published in final edited form as:

J Phys Chem B. 2023 May 25; 127(20): 4633–4645. doi:10.1021/acs.jpcb.3c01025.

The Importance of Nuclear Quantum Effects on the Thermodynamic and Structural Properties of Low-Density Amorphous Ice: A Comparison with Hexagonal Ice

Ali Eltareb,

Department of Physics, Brooklyn College of the City University of New York, Brooklyn, New York 11210, United States; Ph.D. Program in Physics, The Graduate Center of the City University of New York, New York, New York 10016, United States

Gustavo E. Lopez,

Department of Chemistry, Lehman College of the City University of New York, Bronx, New York 10468, United States; Ph.D. Program in Chemistry, The Graduate Center of the City University of New York, New York, New York 10016, United States

Nicolas Giovambattista

Department of Physics, Brooklyn College of the City University of New York, Brooklyn, New York 11210, United States; Ph.D. Program in Physics, The Graduate Center of the City University of New York, New York, New York 10016, United States; Ph.D. Program in Chemistry, The Graduate Center of the City University of New York, New York, New York 10016, United States

Abstract

We study the nuclear quantum effects (NQE) on the thermodynamic properties of low-density amorphous ice (LDA) and hexagonal ice (I_h) at $P = 0.1$ MPa and $T \geq 25$ K. Our results are based on path-integral molecular dynamics (PIMD) and classical MD simulations of H_2O and D_2O using the q-TIP4P/F water model. We show that the inclusion of NQE is necessary to reproduce the experimental properties of LDA and ice I_h. While MD simulations (no NQE) predict that the density $\rho(T)$ of LDA and ice I_h increases monotonically upon cooling, PIMD simulations indicate the presence of a density maximum in LDA and ice I_h. MD and PIMD simulations also predict a qualitatively different T-dependence for the thermal expansion coefficient $\alpha_P(T)$ and bulk modulus $B(T)$ of both LDA and ice I_h. Remarkably, the $\rho(T)$, $\alpha_P(T)$, and $B(T)$ of LDA are practically identical to those of ice I_h. The origin of the observed NQE is due to the delocalization of the H atoms, which is identical in LDA and ice I_h. H atoms delocalize considerably (over a distance ≈

Corresponding Authors gustavo.lopez1@lehman.cuny.edu, ali.eltareb@brooklyn.cuny.edu, ngiovambattista@brooklyn.cuny.edu.

ASSOCIATED CONTENT

Supporting Information

The Supporting Information is available free of charge at https://pubs.acs.org/doi/10.1021/acs.jpcb.3c01025.

Additional results from PIMD simulations of H_2O and D_2O in LDA and ice I_h. Specifically, we (i) explore the sensitivity of our findings to the PIMD simulation time step dt and the number of beads per ring-polymer n_b; (ii) include snapshots of H_2O in LDA showing the corresponding atoms delocalization at different temperatures; and (iii) include the PIMD simulation results for D_2O in both ice I_h and LDA (PDF)

Complete contact information is available at: https://pubs.acs.org/10.1021/acs.jpcb.3c01025

The authors declare no competing financial interest.

20−25% of the OH covalent-bond length) and anisotropically (preferentially perpendicular to the OH covalent bond), leading to less linear hydrogen bonds HB (larger HOO angles and longer OO separations) than observed in classical MD simulations.

Graphical Abstract

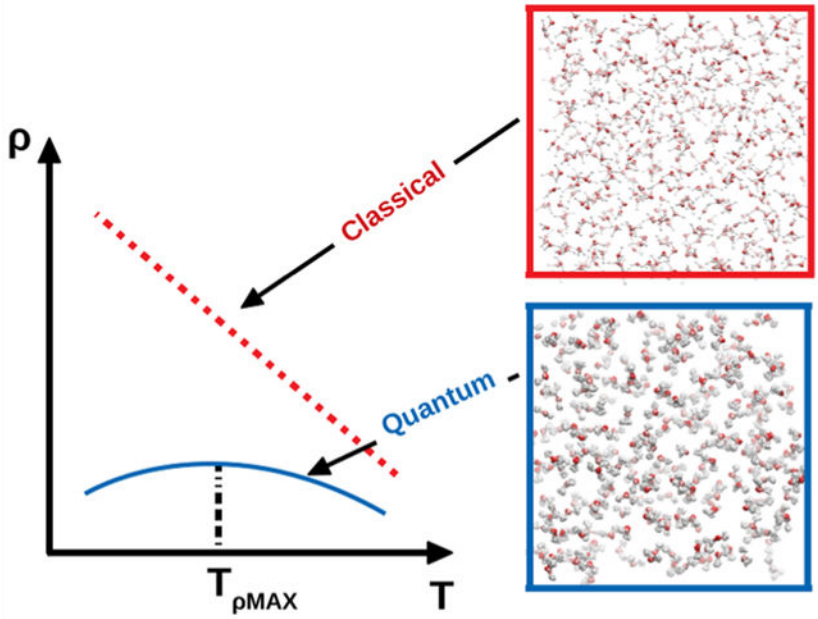

1. INTRODUCTION

Water is one of the most important substances on Earth. It plays a central role in numerous scientific and engineering applications,[1–3] and most biological process in nature occur in liquid water. Curiously, water is also one of the most complex substances known. For example, there are more than 20 forms of ice[4–7] and two different liquid states of water at low temperatures.[8,9] In the out-of-equilibrium glassy state, water exhibits polyamorphism; the two most common forms of glassy water being low-density and high-density amorphous ice (LDA and HDA, respectively).[10–12] Interestingly, the most common form of water in the universe is LDA (more specifically, amorphous solid water, ASW).[13–15] In the laboratory, LDA can be prepared at $P = 0.1$ MPa and approximately $T < 130$ by different routes, including hyperquenching the liquid[14,16] and by vapor deposition on a cold substrate.[17]

Most computational studies of water usually focus on the liquid state, with emphasis on thermodynamic, dynamic, and/or structural properties. Studies of water at low temperatures, in the ice I_h and glassy states, are also available but are less common. Yet, understanding the behavior of glassy water and ice I_h is important for cryogenic applications, including X-ray diffraction experiments of protein crystals[18,19] and cryopreservation techniques. For example, in the cryopreservation of biomolecules and cells, a major problem is the formation of ice crystals which can damage the sample of interest.[20] In such cases, any water volume in the sample needs to be kept in a glassy state.[21] Most computational studies of glassy water have been performed employing (i) classical MD simulations using (ii) rigid water

models, such as SPC/E,[22] ST2,[23,24] and TIP4P/2005.[25,26] In these studies, the properties of LDA/HDA and the phenomenology associated with the LDA-HDA transformation are reproduced qualitatively well, relative to experiments, but differences among the studied water models can be relevant.[27,28] Importantly, classical MD simulations neglect the quantum fluctuations due to the nuclear quantum effects (NQE; i.e., delocalization of atoms) at low temperatures. This can be troublesome because the H atoms of water have a small mass and, hence, they are susceptible to NQE even at moderate temperatures.[29] For example, NQE are responsible for the difference in the melting temperature of H_2O and D_2O ($\delta T \approx 4$ K) as well as in the corresponding temperature of maximum density ($\delta T \approx 7$ K) and the glass transition temperature ($\delta T \approx 10$ K).[30] In addition, computer simulations of water-like models, show that the inclusion of NQE can have a significant impact on the thermodynamic, dynamical, and structural properties of the low-temperature liquid as well as the glass state.[31–33] At present, the role of NQE on LDA and HDA remains poorly understood.

In this work, we perform path-integral molecular dynamics (PIMD) and classical MD simulations of LDA and ice I_h using the q-TIP4P/F model,[34] a realistic water model that has been explicitly parametrized for PIMD simulations. The main goal of this work is (i) to determine the role of NQE (due to atoms delocalization) on the thermodynamic and structural properties of LDA and ice I_h, for both H_2O and D_2O, and (ii) to interpret the different results obtained from classical MD/PIMD simulations (without/with the inclusion of NQE) at the molecular level. Briefly, we show that the inclusion of NQE is necessary to reproduce the structural and thermodynamic properties of ice I_h [specifically, density $\rho(T)$, thermal expansion coefficient $\alpha_P(T)$, and bulk modulus $B(T)$]; similar conclusions hold for LDA. For example, PIMD simulations are consistent with the presence of a weak density maximum in LDA and ice I_h for both H_2O and D_2O, which is absent in the classical MD simulations. A density maximum in ice I_h was reported in experimental[35,36] and theoretical/computational studies[37–39] of H_2O and D_2O ice I_h; at the present time, a density maximum in LDA has not been observed in experiments. Interestingly, the $\rho(T)$, $\alpha_P(T)$, and $B(T)$ of LDA at low temperatures are very similar, if not identical, to those of ice I_h. The discrepancies found between classical MD and PIMD simulations are due to the delocalization of the H atoms. At $T = 25 - 150$ K, the uncertainty in the H location is approximately 0.20−0.25 Å, i.e., 20−25% of the OH covalent-bond length. The H delocalization occurs preferentially along the direction perpendicular to the corresponding OH covalent bond. This leads to less linear hydrogen bonds (HB; larger HOO angles and longer OO separations) than found in classical MD simulations. These NQE are not only evident in the thermodynamic properties studied, but also in the structure of water, as quantified by the radial distribution functions. However, the H atom delocalization barely affects the local tetrahedral order of ice I_h and LDA. This study complements previous works[34,37,40–42] that explore the NQE on the thermodynamic, dynamics, and structural properties of q-TIP4P/F water, H_2O and D_2O, in the liquid state. Compared to the NQE reported in liquid water at $T > 240$ K ($P = 0.1$ MPa),[40,41] the NQE reported here for LDA and ice I_h are profound.

This work is organized as follows. In section II we present the computer simulation details. In section III we discuss the results of our PIMD and classical MD simulations for H_2O using the q-TIP4P/F water model. The corresponding results for D_2O are included in the Supporting Information. A summary is included in section IV.

II. SIMULATION METHOD

We perform classical molecular dynamics (MD) and path-integral molecular dynamics (PIMD) simulations of ice I_h and LDA at $P = 0.1$ MPa; simulations are performed for both H_2O and D_2O. All MD/PIMD simulations are based on the q-TIP4P/F water model,[34] a flexible water model based on the rigid TIP4P/2005 model,[43] which has been used extensively in classical MD simulations. The q-TIP4P/F water model incorporates intramolecular flexibility by modeling the O−H covalent bond potential energy with a fourth order polynomial expansion of a Morse potential and a simple harmonic potential to model the potential energy of the HOH angle. The q-TIP4P/F water model has been optimized to be used in PIMD simulations, and it reproduces remarkably well the properties of liquid water and ice I_h at $P = 0.1$ MPa.[34,40,42,44] All of our MD/PIMD simulations are based on a rectangular or cubic system (ice I_h and LDA, respectively) with periodic boundary conditions at constant temperature and pressure; simulations are performed using the OpenMM (version 7.4.0) software package.[45]

Our PIMD simulations of ice I_h are based on a system composed of $N = 1024$ molecules, where each atom is represented by a ring-polymer composed of n_b beads. Most of the results reported here are for the case $n_b = 128$, but additional simulations at low temperatures are also performed at $n_b = 32 - 300$ (see below). PIMD simulations of ice I_h are performed at temperatures in the range $T = 25 - 300$ K (at $P = 0.1$ MPa). This temperature range includes the equilibrium and metastable states of q-TIP4P/F ice I_h since the melting temperature of q-TIP4P/F water reported from PIMD simulations is $T_M = 251\ K$.[34] A stochastic (local) path integral Langevin equation (PILE) thermostat[46] is used to keep the temperature of the system constant, while a Monte Carlo barostat is used to maintain the pressure at $P = 0.1$ MPa. The thermostat collision frequency used during the equilibration and production runs is set to $\gamma = 1.0\ ps^{-1}$. Short-range (Lennard-Jones pair potential) interactions are calculated using a cutoff $r_c = 1.0$ nm and long-range electrostatic interactions are computed using the reaction field technique[47] with the same cutoff r_c. In the reaction field technique, the dielectric constant (relative permittivity) of the continuum beyond the cutoff radius r_c is set to 78.3. The expression for the reaction field equation implemented in the OpenMM software package to model electrostatic interactions is given in eq 18.6.3 of ref 45. At a given T, the system is equilibrated for 0.5 ns, followed by a production run of 1.5 ns; the simulation time step is 0.25 fs ($n_b \leq 128$) and 0.10 fs ($n_b > 128$).

In order to generate LDA, we perform MD/PIMD cooling simulations starting from equilibrium liquid water configurations obtained at $T = 240$ K and $P = 0.1$ MPa. Specifically, in these simulations, liquid water is cooled isobarically at $P = 0.1$ MPa down to $T = 25$ K. During these cooling runs, the thermostat temperature is reduced linearly with time, with

a cooling rate of $q_T = 10$ K/ns. This cooling rate is 3 orders of magnitude faster than the estimated slowest experimental rate 0.01 K/ns[48] used to prepare hyperquenched glassy water (HGW),[16] a low-density glass that belongs to the LDA family.[7,20] Cooling rates of $q_T = 10$ K/ns have been used previously in classical MD simulations of water to generate LDA.[25,26,49] To control the temperature, the thermostat collision frequency parameter is set to $\gamma = 1.0\ \text{ps}^{-1}$. As for the case of ice I_h, the time step used in the cooling runs is set to 0.25 fs, and $n_b = 128$. For the isobaric cooling runs, we use a system composed of $N = 512$ water molecules. PIMD simulations are performed for both H_2O and D_2O.

PIMD simulations can be sensitive to technical details, in particular, to the number of beads per ring-polymer employed. In order to test the robustness of our results to variations in n_b, we perform additional PIMD simulations using $n_b = 32$, 72, 128, 256, and 300, for H_2O ice I_h and $n_b = 32$, 72, and 128 for H_2O LDA. Briefly, we find that the reported structural properties and most of thermodynamic properties studied, including the density and thermal expansion coefficient, are robust to variations in n_b. However, minor differences in some of the properties studied, including $\rho(T)$, may remain sensitive to n_b at the lowest temperatures studied, $T = 25$ K. Our results for the enthalpy and, hence, the isobaric heat capacity are sensitive to n_b [see Supporting Information (SI)]. Similar effects of n_b on the various properties studied in this work were reported previously for the case of equilibrium liquid water in ref 40, and additional details can be found there.

All of our classical MD simulations are performed by setting $n_b = 1$ in the PIMD simulations. The same computational details described above hold for the classical simulations except that the time step is increased to $dt = 0.5$ fs.

III. RESULTS

Our results are organized as follows. In section IIIA, we discuss the thermodynamic and structural properties of ice I_h and LDA for the case of H_2O from classical MD and PIMD simulations, and compare the simulation results with available experimental data. Section IIIB focuses on the local order and hydrogen bonding of H_2O in the LDA and ice I_h states, including the local tetrahedrality of the corresponding HB-network and geometrical properties of the HBs. The delocalization of water O and H atoms in LDA and ice I_h is discussed in section IIIC. The corresponding results for D_2O are included in the SI.

A. Thermodynamic and Structural Properties of LDA and Ice I_h.

A.1. Density.—Figure 1 shows the densities of ice I_h at $P = 0.1$ MPa and $T = 25 - 300$ K obtained from PIMD and classical MD simulations using the q-TIP4P/F water model (blue circles). For comparison, also included are the experimental densities of ice I_h from ref 35 (brown circles). The densities of ice I_h obtained from PIMD simulations are in remarkably good agreement with the experiments (Figure 1a). The deviations between the PIMD simulations and experiments are less than 0.5%. Instead, the densities of ice I_h from classical MD simulations are off relative to the experimental values by 4% (Figure 1b). In particular, we note that only the PIMD simulations, which include NQE, predict an apparent saturation

in the density of ice I_h at low temperatures, consistent with experiments.[35] Instead, classical MD simulations misleadingly predict a monotonic increase in density upon cooling.[25,26] Our results for ice I_h in Figure 1a are fully consistent with the studies of Herrero and Pamuk[37,38] who studied the density of ice I_h using PIMD simulations with the q-TIP4P/F water model. In the experiments of ref 35 (brown circles in Figure 1a) and the simulations of refs 37 and 38, a very weak density maximum in ice I_h is identified at low temperatures for both H_2O and D_2O. Our results in Figure 1a for H_2O and Figure S5(a) for D_2O are also consistent with the presence of a weak density maximum in ice I_h at $T \approx 100$ K.

The red circles in Figure 1a,b are the densities of q-TIP4P/F water upon cooling the liquid from $T = 240$ K down to $T \leq 35$ K, into the glass (LDA) state (cooling rate of $q_T = 10$ K/ns). During the isobaric cooling process, both classical MD and PIMD simulations show that the density of liquid water initially decreases down to approximately $T = 180 - 200$ K while at lower temperatures H_2O vitrifies into LDA.[25,26,50] The experimental densities of LDA at $T = 80$ and 140 K reported in refs 12 and 51, are also included in Figure 1a,b (magenta and orange squares). Importantly, as for the case of ice I_h, only the PIMD simulations are able to reproduce the experimental densities of LDA.

The densities for LDA predicted by the PIMD and classical MD simulations are considerably different at low temperatures. Specifically, during the isobaric coolings of H_2O, classical MD simulations indicate that the density of q-TIP4P/F water increases monotonically at $T < 180$ K, while water remains in the LDA state. Instead, PIMD simulations show that the density of LDA saturates at low temperatures. Indeed, a very weak density maximum can be observed in H_2O LDA at $T \approx 100$ K, i.e., at the same temperature at which H_2O ice I_h seems to exhibit a density maximum. Note that the $\rho(T)$ for LDA and ice I_h, are remarkably close to one another. This is probably due to the highly tetrahedral local structure of ice I_h and LDA (see section IIIB). Interestingly, our PIMD simulations of D_2O are also consistent with the presence of a density maximum in LDA and ice I_h at $T \approx 100$ K; see Figure S5(a) of the SI.

A.2. Thermal Expansion Coefficient and Bulk Modulus.—The thermal expansion coefficient and bulk modulus are among the most important thermodynamic response functions used to characterize solids. We discuss first the thermal expansion coefficient of LDA and ice I_h, and then, we focus on the corresponding bulk modulus.

The thermal expansion coefficient is defined as

$$\alpha_P(T) = \frac{1}{V}\left(\frac{\partial V}{\partial T}\right)_P \quad (1)$$

The $\alpha_P(T)$ of ice I_h obtained from PIMD and classical MD simulations using the q-TIP4P/F water model are shown in Figure 2a at $P = 0.1$ MPa (solid red and blue lines, respectively).[52] Also included is the experimental $\alpha_P(T)$ of ice I_h from ref 35 (brown circles). PIMD simulations (red solid line) are able to reproduce remarkably well the experimental $\alpha_P(T)$ of ice I_h at $T < 200$ K and almost exactly at $T < 50$ K. Instead, the $\alpha_P(T)$ obtained from

classical MD simulations are considerably off from the experimental values. It follows that the inclusion of NQE is necessary to reproduce the experimental thermal expansion coefficient of ice I_h.

To the best of our knowledge, the experimental $\alpha_P(T)$ of LDA is not known. Figure 2(a) shows the $\alpha_P(T)$ of q-TIP4P/F water obtained during the isobaric cooling runs at $P = 0.1$ MPa where the equilibrium liquid is vitrified into LDA. Interestingly, both PIMD and classical MD simulations indicate that the $\alpha_P(T)$ of LDA and ice I_h are remarkably similar to each other. However, the results from classical MD and PIMD simulations are considerably different implying that, consistent with Figure 1, NQE should not be omitted when studying the thermodynamic properties of ice I_h/LDA.

As shown in Figure 1, experiments and PIMD simulations (but not classical MD simulations) are consistent with ice I_h exhibiting an anomalous density maximum at $T_{\rho,\max} \approx 75$ K and $T_{\rho,\max} \approx 100$ K, respectively. Accordingly, it must be that $\alpha_P(T) = 0$ at $T = T_{\rho,\max}$, while $\alpha_P(T) > 0$ at $T > T_{\rho,\max}$ and $\alpha_P(T) < 0$ at $T < T_{\rho,\max}$. Indeed, this is confirmed by the $\alpha_P(T)$ obtained from experimental and PIMD simulations shown in Figure 2a. The same conclusions follow from the PIMD simulations of LDA for which $T_{\rho,\max} \approx 100$ K (again, the maximum density in LDA and ice I_h occurs at roughly the same temperature).

We note that, from the statistical mechanics point of view, the thermal expansion coefficient is a measure of the correlations between the entropy and volume fluctuations, i.e., $\alpha_P(T) = \frac{\langle \Delta S \Delta V \rangle}{V k_B T}$[53] It follows from Figure 2a that, at $T < T_{\rho,\max}$, the correlations between the volume and entropy of ice I_h and LDA are anomalously negative. Therefore, at these temperatures, a fluctuation in H_2O, in either the ice I_h or LDA state, that increases the volume of the system should be accompanied by an entropy fluctuation that decreases the entropy of system and vice versa. This anomalous anticorrelation between the entropy and volume fluctuations for ice I_h and LDA is reminiscent of the behavior found in liquid water, for which the density maximum temperature is $T_{\rho,\max} = 277$ K.[53] Again, the origin of such an anticorrelation in the entropy-volume fluctuations of ice I_h and LDA is a consequence of NQE since this kind of anticorrelations in entropy-volume fluctuations is not found in the classical MD simulations (using the q-TIP4P/F water model).

Next, we turn our attention to the bulk modulus of ice I_h and LDA,

$$B(T) = -V\left(\frac{\partial P}{\partial V}\right)_T \tag{2}$$

Since $B(T) = 1/\kappa_T(T)$, where $\kappa_T(T)$ is the isothermal compressibility of the system, it follows that $B(T)$ is related to the volume fluctuations of the system.[54] Specifically,

$$B(T) = \frac{k_B T \langle V \rangle}{\langle V^2 \rangle - \langle V \rangle^2} \tag{3}$$

where $\langle \cdots \rangle$ indicates the average over configurations and k_B is the Boltzmann's constant. In this work, we calculate $B(T)$ (at $P = 0.1$ MPa) using eq 3.

The $B(T)$ of ice I_h obtained from PIMD and classical MD simulations using the q-TIP4P/F water model are shown in Figure 2b. For comparison we have also included in Figure 2b, experimental values of $B(T)$ for ice I_h from ref 55 (brown circles). The values of $B(T)$ from PIMD simulations for ice I_h overlap with the experimental $B(T)$ throughout the entire temperature interval. Instead, the $B(T)$ calculated from classical MD simulations agrees with the experimental values at only $T \geq 150$ K. At lower temperatures, classical MD simulations overestimate $B(T)$ by approximately 5 GPa. This is another indication that NQE cannot be omitted when studying the thermodynamic properties of ice I_h at low temperatures.

It follows from eq 3 and Figure 2b that only PIMD simulations are able to reproduce the volume fluctuations of ice I_h at all temperatures. In other words, only when the delocalization of water atoms are included, the experimental volume-fluctuations of ice I_h are reproduced. It may seem counterintuitive that the same conclusions do not hold for the case of liquid water ($P = 0.1$ MPa). As we showed in ref 40, PIMD simulations of q-TIP4P/F liquid water at $T < 250$ K are considerably underestimated, relative to real water.

To the best of our knowledge, the experimental bulk modulus of LDA is not known. Figure 2b shows the bulk modulus of q-TIP4P/F water obtained during the cooling-induced liquid-to-LDA transformation. Interestingly, the $B(T)$ obtained during the cooling runs performed using MD and PIMD simulations are in full agreement with one another. The main point of Figure 2b is that the $B(T)$ of LDA and ice I_h overlap (see Figure 2b for $T < 180$ K).

A.3. Radial Distribution Function.—In order to further explore the role of NQE on ice I_h and LDA, we discuss next the radial distribution function (RDF) of H_2O obtained from the MD and PIMD simulations. The oxygen−oxygen (OO) RDF of q-TIP4P/F water in the ice I_h and LDA states are shown in Figure 3. Included are the RDF from PIMD and classical MD simulations, as well as experiments. The OO RDF from PIMD/MD simulations are very similar to each other and are in good agreement with experiments. The main differences are found at $r = 2.8$ Å, where the first peak of the OO RDF is located. Specifically, relative to the experiments, both PIMD and classical MD simulations overestimate the height of the OO RDF first peak, predicting a more structured ice I_h and LDA than found in experiments. However, the PIMD simulations do a better job than the classical MD simulation, i.e., the inclusion of NQE leads to a reduction in the OO RDF first peak, closer to the experimental observations. Also shown in Figure 3, are the OH and HH RDF of H_2O obtained from MD and PIMD simulations for LDA and ice I_h. Similar to the OO RDF, the OH and HH RDF maxima become smaller once NQE are included; however, the corresponding peak positions are not changed.

The reduction of the OO RDF maxima is known to occur when NQE are included.[40] For example, in liquid water at $T = 220$ K and $P = 0.1$ MPa, the height of the OO RDF first peak is $g_1^C = 4.6$, from classical MD simulations, while $g_1^Q = 4.0$ from PIMD simulations (see Figure 9(a) in ref 40). Hence, including NQE leads to a reduction in the height of the

OO RDF first peak of $R_{C/Q} = g_1^C/g_1^Q = 1.15$. For comparison, we note that $R_{C/Q} = 1.49$ in the case of ice I_h (Figure 3b), and $R_{C/Q} = 1.38$ in the case of LDA (Figure 3a). Therefore, as one may expect, the inclusion of NQE on the OO RDF becomes more pronounced at low temperatures. We note that, as shown in the SI (Figure S6), the inclusion of NQE has similar effects in the OO RDF of D_2O, leading to less structured ice I_h and LDA relative to classical MD simulations.

B. Local Structure and Hydrogen Bonds in LDA and Ice I_h.

B.1. Local Order Parameters.—

In this section, we characterize the local structure of LDA and ice I_h from classical MD and PIMD simulations of H_2O (q-TIP4P/F model) using two local order metrics, the tetrahedral order parameter $\langle q \rangle$,[58] and the $\langle d_{fs} \rangle$ order parameter introduced in ref 59. The local order parameter $\langle q \rangle$ depends only on the first hydration shell of the water molecules; the parameter $\langle d_{fs} \rangle$ quantifies the local order of a given water molecule at distances in between its first and second hydration shells.

The local order parameter q_i of molecule i is given by,[58]

$$q_i = 1 - \frac{3}{8} \sum_{j=1}^{3} \sum_{k=j+1}^{4} \left(\cos(\Psi_{ijk}) + \frac{1}{3} \right)^2 \tag{4}$$

where Ψ_{ijk} is the angle formed by the lines joining the O atom of molecule i and the O atoms of its nearest neighbors j and k. In classical MD simulations, the average local order parameter of the system, $\langle q \rangle$, is obtained by averaging q_i over all molecules $i = 1, 2, \ldots, N$ and over time. In the PIMD simulations, the local order parameter for molecule i is calculated by averaging over all replicas in the system, i.e.,

$$q_i = \frac{1}{n_b} \sum_{k=1}^{n_b} q_{i,k} \tag{5}$$

where $q_{i,k}$ is given by eq 4 with all O atoms belonging to replica k (n_b is the number of beads per ring-polymer, it is also the number of replicas in the system). The tetrahedral order parameter of the system, $\langle q \rangle$, is the average of q_i over all molecules $i = 1, 2, \ldots, N$ and over time, as done in the case of classical MD. We note that $\langle q \rangle = 1$ for a perfect tetrahedral network such as the case of ice I_h; instead, $\langle q \rangle = 0$ for a random distribution of molecules.

Figure 4a shows $\langle q \rangle$ as a function of temperature for H_2O in ice I_h and during the isobaric cooling of liquid water into LDA. The results from PIMD and classical MD simulations are very close to one another. The only (minor) differences in Figure 4a between classical MD and PIMD simulations are observable in the case of ice I_h at low temperatures; specifically, the local tetrahedral order for ice I_h (red/blue circles) is slightly smaller when NQE are introduced.

Classical MD and PIMD simulations show that the $\langle q \rangle$ of both ice I_h and LDA increase as the system is cooled, indicating that the water molecules are in increasingly more tetrahedral

environments as the temperature decreases. As expected, at very low temperatures ($T < 50$ K), ice I_h is almost perfectly tetrahedral, with $\langle q \rangle = 0.96 - 0.98$. LDA is also highly tetrahedral, but slightly less than ice I_h, with $\langle q \rangle = 0.87 - 0.88$ ($T < 50$ K).

Next, we focus on the local order of water molecules about their second hydration shell, as quantified by the order parameter $\langle d_{fs} \rangle$.[59] For a given molecule i, $d_{i,fs}$ is defined as the difference between (a) the (OO) distance from molecule i to its 5th neighbor, and (b) the (OO) distance from molecule i to its 4th neighbor. In classical MD simulations, $\langle d_{fs} \rangle$ is obtained by averaging $d_{i,fs}$ over all molecules $i = 1, 2, \ldots, N$ and over time. Similarly to the tetrahedral order parameter $\langle q \rangle$, the definition of $\langle d_{fs} \rangle$ can be easily generalized to the case of PIMD simulations by first calculating $d_{i,fs}$ over the replicas of the system. Specifically, in the PIMD simulations, the order parameter for molecule i is calculated by averaging over all replicas in the system, i.e.,

$$d_{fs}^{i} = \frac{1}{n_b} \sum_{k=1}^{n_b} d_{fs}^{i,k} \tag{6}$$

where $d_s^{i,k}$ is calculated from all O atoms belonging to replica $k = 1, 2, \ldots, n_b$. As for the classical MD case, $\langle d_{fs} \rangle$ is the average of d_{fs}^{i} over all molecules $i = 1, 2, \ldots, N$ and over time. We note that the minimum value of $\langle d_{fs} \rangle$ for water is 0, corresponding to the full migration of a water molecule from the second hydration shell to the first hydration shell of a given water molecule. Accordingly, small values of $\langle d_{fs} \rangle$ imply that water molecules are in a HDL/HDA-like local environment. The largest value of $\langle d_{fs} \rangle$ is ≈1.5 Å corresponding to empty first interstitial shells. Accordingly, large values of $\langle d_{fs} \rangle$ (e.g., $\langle d_{fs} \rangle > 0.6$ Å) indicate that water molecules are in an LDL/LDA-like arrangement.

The values of $\langle d_{fs} \rangle$ obtained from PIMD and classical MD simulations for H_2O are shown in Figure 4b. The temperature dependence of $\langle d_{fs} \rangle$ and $\langle q \rangle$ are remarkably similar. Briefly, for both ice I_h and LDA, $\langle d_{fs} \rangle$ increases as the temperature decreases, which indicates that the separation between the first and second hydration shells of the water molecules become more pronounced at low temperatures. The introduction of NQE in the PIMD simulations leads to slightly smaller values of $\langle d_{fs} \rangle$ relative to the classical MD simulations, for both ice I_h and LDA. Interestingly, in the PIMD simulations, $\langle d_{fs} \rangle$ seems to reach a plateau at $T < 100$ K, i.e., at the same temperature at which $\rho(T)$ of LDA and ice I_h saturates (Figure 1a). It follows that at $T < 100$ K, and in the presence of NQE, the distance between the first and second shells of the water molecule remains approximately constant. Instead, classical MD simulations show a monotonic increase $\langle d_{fs} \rangle$ upon cooling at low temperatures, which is consistent with the monotonic increase of $\rho(T)$ at $T < 100$ K.

B.2. Hydrogen Bonds.—Water molecules in the liquid or solid state form approximately four hydrogen bonds (HB) with their nearest neighbors. Here, we characterize the HB between water molecules in ice I_h and LDA. Specifically, for a given pair of water molecules forming a HB, we study (i) the OO distance between the corresponding O atoms, $d_{OO}^{HB}(T)$, and (ii) the HOO angle, $\theta_{HOO}^{HB}(T)$, formed by the corresponding

O-to-H covalent bond (associated with the donor O atom) and the vector pointing from the donor O atom to the acceptor O atom. In this work, we use the geometrical definition of HB from ref 60, where two water molecules form a HB if the corresponding OO distance is less than 3.5 Å and the HOO angle is less than 30°.

Figure 5a shows the $\langle d_{OO}^{HB}(T)\rangle$ during the cooling-induced liquid-to-LDA transformation at $P = 0.1$ MPa from PIMD (red lines) and classical MD simulations (blue lines) and experiments (black squares). PIMD simulations are able to reproduce remarkably well the experimental values of $d_{OO}^{HB}(T)$, while classical MD simulations predict a slightly shorter OO distance, off by ≈0.02 Å from the experimental value. Accordingly, the inclusion of NQE brings the simulation results closer to the corresponding experimental observations. The main differences between the PIMD and classical MD simulations occur at low temperatures. The inclusion of NQE leads to a saturation in $\langle d_{OO}^{HB}(T)\rangle$ at approximately $T < 100$ K while, instead, classical MD simulations predict a monotonic decrease of the $\langle d_{OO}^{HB}(T)\rangle$ upon cooling. One would expect that the density of ice I_h/LDA increases as $\langle d_{OO}^{HB}(T)\rangle$ decreases, (and vice versa), i.e., as the molecules forming a HB get closer to one another. A comparison of Figures 1 and 5a shows that this is indeed supported by our classical MD/PIMD simulations. Specifically, in the case of classical MD, $\langle d_{OO}^{HB}(T)\rangle$ decreases, while $\rho(T)$ increases, monotonically upon cooling at low temperature. Instead, in the case of PIMD simulations, $\langle d_{OO}^{HB}(T)\rangle$ saturates at low temperatures. A minimum in the $\langle d_{OO}^{HB}(T)\rangle$ of LDA cannot be resolved within the resolution of our data.

Consistent with these conclusions, the OO distance between hydrogen-bonded water molecules in ice I_h differs in MD and PIMD simulations; see the blue and red solid circles in Figure 5a. Specifically, upon cooling, classical MD (blue lines) predicts that $\langle d_{OO}^{HB}(T)\rangle$ decreases monotonically upon cooling while, instead, PIMD simulations (red lines) indicate that $\langle d_{OO}^{HB}(T)\rangle$ exhibits a very weak, wide minimum in the $\langle d_{OO}^{HB}(T)\rangle$ at $T \approx 80$ K, close to the temperature at which the density $\rho(T)$ of ice I_h shows a very weak maximum. This strongly suggests that the density maximum in ice I_h, and possibly LDA, is due to the NQE on the HB of water, which leads to a minimum in the OO distance at low temperature. The density maximum in ice I_h, can also be explained by the existence of low frequency vibrational modes in ice I_h that have a negative Grüniesen parameter.[39,61]

Figure 5b shows the HOO angle between two water molecules in ice I_h and during the cooling-induced vitrification of liquid water into LDA ($P = 0.1$ MPa). In both cases, the qualitative behavior of $\langle \theta_{HOO}^{HB}(T)\rangle$ is similar to the behavior of $\langle d_{OO}^{HB}(T)\rangle$ shown in Figure 5a. Specifically, for both ice I_h (red circles) and LDA (red lines), introducing NQE increases the values of $\langle \theta_{HOO}^{HB}(T)\rangle$ by a factor of ≈2 relative to the classical MD simulations prediction (blue circles and lines). Hence, including the delocalization of the H atoms leads to less linear HB (larger $\langle \theta_{HOO}^{HB}(T)\rangle$) between water molecules. Interestingly, we note that these NQE on the HB network of water do not alter the local tetrahedrality order of the system (see Figure 4a).

It also follows from Figure 5b that the qualitative behavior of $\langle \theta_{HOO}^{HB}(T)\rangle$ is different in classical MD and PIMD simulations. As for the case of $\langle d_{OO}^{HB}(T)\rangle$, classical MD simulations

predict that the $\langle \theta_{HOO}^{HB}(T) \rangle$ decreases monotonically with decreasing temperature, in both ice I_h and during the vitrification of liquid water into LDA. Instead, PIMD simulations indicate that $\langle \theta_{HOO}^{HB}(T) \rangle$ saturates at around $T \approx 100$ K. Again, the different behaviors in the $\langle \theta_{HOO}^{HB}(T) \rangle$ obtained from MD/PIMD simulations are consistent with the corresponding behaviors in $\rho(T)$ for both ice I_h and during the vitrification of liquid water into LDA.

C. Delocalization of the Ring-Polymers of Ice I_h and LDA.

In order to quantify the quantum delocalization of the water O and H atoms in ice I_h and LDA, we calculated the average radius of gyration of the corresponding ring-polymers R_g. The radius of gyration for a given ring-polymer is defined as

$$R_g = \left\langle \frac{1}{n_b} \sum_{i=1}^{n_b} (r_c - r_i)^2 \right\rangle \quad (7)$$

where r_c is the center of mass (centroid) of the given ring-polymer and r_i is the position of the ring-polymer bead i; the $\langle \cdots \rangle$ indicate an average over time and over all ring-polymers in the system. It can be shown within the PI formalism of statistical mechanics that the R_g of a given ring-polymer is related to the quantum mechanics uncertainty in the position of the associated atom.[63]

The R_g of the O and H atoms of water in ice I_h and during the cooling-induced liquid-to-LDA transformation ($P = 0.1$ MPa) are shown in Figure 6b. Consistent with previous computational studies performed on water-like models,[32] $R_g(T)$ increases as the temperature is decreased (i.e., the O and H atoms become increasingly delocalized upon cooling at lower temperatures). The delocalization of the H atoms in ice I_h and LDA is considerable. For example, at $T = 80$ K, R_g is approximately 0.20 Å, which corresponds to 20% of the OH covalent bond length. Not surprisingly, the O atoms are less delocalized than the H atoms since NQE are less important for heavy atoms.

Interestingly, the R_g values obtained from our PIMD simulations for the O and H ring-polymers in ice I_h and liquid/LDA overlap throughout the entire temperature range, implying that the delocalization of the H and O atoms in LDA and ice I_h are identical. This can be understood by noticing that LDA and ice I_h have a similar local tetrahedral structure (see Figure 4a). To test whether the delocalization of the O and H atoms is a property of the water molecules, i.e., independent of the local molecular environment, we also calculate the R_g of the O and H atoms in the low density vapor phase (magenta triangles). As shown in Figure 6b, the O and H atoms are more delocalized in the vapor phase than in ice I_h or LDA and hence, the delocalization of the water atoms does depend on the local environment ($P = 0.1$ MPa).

The radius of gyration R_g quantifies the average spread of the O and H ring-polymers, but it provides no information on whether such a spreading is anisotropic. In order to elucidate whether there is a preferential direction for the O and H atom delocalization, we also calculate the delocalization of the atoms along specific axes that are fixed at the

corresponding water molecules. Specifically, for a given molecule, we define the x-, y-, and z-axes indicated in Figure 6a. In Figure 6a, the origin of the x-y-z reference frame associated with the given water molecule is located on the O centroid (ring-polymer center of mass). The z-axis is perpendicular to the plane containing the centroids of the H_1, O, and H_2 atoms and the x-axis is along the $\overrightarrow{R}_{OH_1}$ vector direction; the y-axis is perpendicular to the x- and z-axis, as shown in Figure 6a, and it is slightly off the $\overrightarrow{R}_{OH_2}$ vector direction. In order to quantify the O and H atoms delocalization along the x-, y-, and z-axis, we define,

$$R^2_{g,\alpha} = \frac{1}{n_b}\sum_{i=1}^{n_b}\left(\overrightarrow{r}_{c,\alpha} - \overrightarrow{r}_{i,\alpha}\right)^2 \quad (8)$$

where $\overrightarrow{r}_c$ and $\overrightarrow{r}_i$ are the vector position of the ring-polymer centroid and bead i, respectively, and α indicates the corresponding vector component $\alpha = x$, y, and z. It follows that $R^2_g = R^2_{g,x} + R^2_{g,y} + R^2_{g,z}$. Figure 6c,d shows $R^2_{g,x}$ and $R^2_{g,z}$ for the O and H_1 ring-polymers in ice I_h and during the cooling-induced liquid-to-LDA transition ($P = 0.1$ MPa). Results for H_2 are, as expected, identical to those found in H_1. We do not show $R^2_{g,y}$ in Figure 6 because, in all cases, it is found that $R^2_{g,y} \approx R^2_{g,x}$.

We focus first on the delocalization of the O atoms. As we show next, the O atoms experience a mild, isotropic delocalization, independently of whether water is in the ice I_h, liquid/LDA, or vapor state.[64] The $R^2_{g,x}$ and $R^2_{g,z}$ of the O atoms in ice I_h are indicated by the red triangles in Figure 6c,d; the corresponding results for the O atoms during the liquid-to-LDA transition (red lines) and in the vapor phase (green triangles) are also included. The fact that the red triangles, red lines, and green triangles in Figure 6c,d overlap with one another implies that the delocalization of the O atoms is identical in all these phases of water (vapor, liquid, LDA, and ice I_h). The delocalization of the O atoms is rather small, with $R_{g,x}$, $R_{g,z} \leq 0.07$ Å (7% of the OH covalent bond length), and increases weakly upon cooling. In particular, a comparison of Figure 6c,d, shows that $R^2_{g,x} \approx R^2_{g,z}$ in all cases, meaning that the delocalization of the O atoms is isotropic for water in the vapor, liquid, LDA, and ice I_h states. To confirm this, we include in Figure 7 the snapshots of water molecules obtained from PIMD simulations in ice I_h at different temperatures (snapshots of water molecules in the LDA state are included in Figure S3 of the SI). The beads of the ring-polymer associated with the O atom are distributed isotropically, forming a spherical (red) cloud that increases in size upon cooling. Similarly, Figure 8 shows the contour map for the probability distribution to find the O ring-polymer beads. The contour maps for the O atoms in Figure 8 are circular at all temperatures considered, consistent with the isotropic delocalization of the O atoms (see also section II of the SI).

Next, we focus on the delocalization of the H atoms. Briefly, we find that the H atoms experience a considerable, anisotropic delocalization. The delocalization of the H atoms is identical in the liquid, LDA, and ice I_h states but H atoms are less delocalized than in the low-density vapor phase. The $R^2_{g,x}$ and $R^2_{g,z}$ of the H atoms in ice I_h are indicated by the blue triangles in Figure 6c,d, while the corresponding $R^2_{g,x}$ and $R^2_{g,z}$ during the liquid-to-LDA transition are indicated by blue lines; the results for the H atoms in the vapor phase are

represented by the magenta triangles. The fact that the blue triangles and blue lines overlap in Figure 6c,d implies that the delocalization of the H atoms is identical in the ice I_h and in the liquid/LDA states. In addition, the values of $R^2_{g,x}$ and $R^2_{g,z}$ in the ice I_h/liquid/LDA (blue lines/circles) are smaller than the corresponding values in the vapor phase (magenta triangles), indicating that H delocalization is largest in the vapor phase ($P = 0.1$ MPa). It follows that the delocalization of the H atoms is not a property of the water molecule, but it depends on the molecular local environment. By the same token, the similar delocalization of the H atoms in the liquid, LDA, and ice I_h state at $P = 0.1$ MPa can be understood by noticing that, in these cases, water molecules are located in a rather tetrahedral structure (at approximately $T < 240$ K).

An important point from Figure 6c,d is that the H atoms are delocalized anisotropically. Specifically, for all phases of water considered (vapor, liquid, LDA, and ice I_h), Figure 6c,d indicates that the H_1 atoms of water (Figure 6a) delocalize preferentially along the z-axis, i.e., $R_{g,z} > R_{g,x}$. Hence, since $R_{g,z} > R_{g,x}$, the H atoms delocalization is preferentially along the directions perpendicular to the corresponding HB. This is confirmed from the snapshots of water in ice I_h shown in Figure 7. The (white) cloud of beads associated with the H atoms are stretched preferentially along the directions perpendicular to the corresponding OH covalent-bond direction, and it is centered at the OH covalent-bond direction. Not surprisingly, the anisotropic delocalization of the H atoms becomes more pronounced at low temperatures. Our conclusions are also consistent with Figure 8, which includes the contour map for the probability distribution to find the H_1 ring-polymer beads at a given position. The contour maps for the H_1 atoms in Figure 8 are circular when projected on the $y - z$ plane, but are ellipsoidal when projected on the $x - y$ plane (see reference frame in Figure 6a). Figure 8 shows that the H atoms can be delocalized by up to ≈0.5 Å along the covalent-bond direction and up to ≈0.4 Å along the direction perpendicular to the OH covalent-bond direction.

The results presented in this section are helpful to understand the differences in the HB properties discussed in section IIIB, as observed in the classical MD and PIMD simulations. Specifically, the inclusion of NQE leads to the delocalization of the H atoms along the direction perpendicular to the OH covalent bond, which results in a larger $\theta^{HB}_{HOO}(T)$, relative to the classical MD case (Figure 5b). Interestingly, we note that a similar preferential delocalization is found in D_2O for the D atoms; see Figures S10–S12 of the SI.

IV. SUMMARY AND DISCUSSION

In this work, we studied the NQE on the thermodynamic and structural properties of H_2O in LDA and ice I_h (the results for D_2O are in the SI). Our results obtained from PIMD simulations using the q-TIP4P/F water model, where NQE are included, are in remarkably good agreement with available experimental data. Instead, our classical MD simulation results (based on the same water model) not only deviate from the experimental observation, but predict the qualitatively wrong thermodynamic behavior of ice I_h and LDA at low temperatures. This is evident in the densities of LDA and ice I_h predicted by PIMD/MD simulations shown in Figure 1. Including NQE leads to a weak maximum in the density

of LDA and ice I_h at $T_{\rho max} \approx 100$ K (a weak maximum density in ice I_h has been reported in experiments[35,36]). Instead, classical MD simulations misleadingly predict a monotonic increase in the density of LDA and ice I_h upon cooling (see also refs 37 and 44).

An important result of this work is that the thermodynamic properties of ice I_h and LDA are remarkably similar. Specifically, the density, thermal expansion coefficient, and bulk modulus of ice I_h and LDA overlap within error bars at $T < 150$ K. These observations are of practical relevance since the available experimental data on the thermodynamic properties of LDA at low temperatures is rather limited. The thermodynamic properties of LDA at low temperatures play a fundamental role in ultrafast heating experiments that may be used to identify the liquid−liquid critical point in water. In such experiments, LDA is subject to ultrafast heating using a laser, and the final state of the system after heating depends on the thermodynamic properties of LDA.[8,65] Interestingly, our PIMD simulations are consistent with the presence of a density maximum in LDA at $T \approx 100$ K. Such a maximum is intriguing and requires experimental confirmation. The density maximum in ice I_h and LDA is remarkably weak and requires a high resolution in the density values, on the order of ≈0.0025 g/cm^3 (see Figures 1a and S1(a), and refs 35–38). For comparison, the density maximum in liquid water from experiments and computer simulations extends over a larger density interval, >0.02 g/cm^3.[40] In this regard, it would be useful to perform additional PIMD simulations at $T < 50$ K to reproduce the density maximum reported for ice I_h[37–39] and LDA with a much larger number of beads per ring-polymer than employed here, e.g., $n_b \geq 1000$.

We stress that our simulations are based on a flexible water model, and hence, our results strongly suggest that it is the atoms delocalization, and not just the water flexibility, that is key when studying the thermodynamics of ice I_h and LDA at low temperatures. This is particularly important in the case of glassy water, since most computational studies of amorphous ice have been performed using classical MD simulations of rigid water models.[22–26,49,50,66]

In order to understand the origin of the different thermodynamic behaviors in ice I_h/LDA with and without the inclusion of NQE, we also studied the corresponding structure (OO, OH, and HH RDF) and local order of water. The OO-RDFs obtained from PIMD simulations for H_2O LDA and ice I_h are in excellent agreement with the experimental data. Consistent with previous studies of water in the ice and liquid states, including NQE (PIMD simulations) reduces the height of the RDFs maxima of ice I_h and LDA, relative to the corresponding RDF calculated from classical MD simulations, and brings the computer simulation results closer to the experimental observations. However, the location of the RDF extrema, which specify the hydration shells of water molecules, are not affected by the inclusion of NQE. Similarly, local order metrics, such as the local tetrahedral order of water molecules, are unaffected by the inclusion of atoms delocalization.

Our results indicate that the differences in the thermodynamic and structural properties of ice I_h and LDA predicted by PIMD and classical MD simulations can be traced down to the HB between water molecules. Specifically, the delocalization of the H

atoms becomes important in ice I_h and LDA at low temperatures, with the H atoms delocalizing preferentially along the directions perpendicular to the corresponding OH covalent bond. This results in less linear HB (larger HOO angles, Figure 5b) and larger OO separations (Figure 5a) than found in classical MD simulations. The larger OO separations between hydrogen-bonded molecules, when NQE are present, is consistent with the smaller density on ice I_h/LDA in the PIMD simulations, relative to the classical MD simulations. Importantly, in the case of ice I_h, we observe a minimum in $\langle d_{OO}^{HB}(T)\rangle$ at temperatures close to the corresponding density maximum. The less linear HB when NQE are present explains why ice I_h and LDA are less structured (see Figure 5b) in PIMD simulations than in classical MD simulations. We also note that the similar thermodynamic properties of ice I_h and LDA are fully consistent with the practically identical HB properties in ice I_h/LDA. The remarkably similar delocalization of the H atoms in ice I_h and LDA can be understood by noticing that, in both cases, water molecules are arranged in highly tetrahedral environments with roughly four HB per water molecule.

We conclude this section by commenting on the role of NQE in the properties of liquid water. Interestingly, while PIMD simulations of q-TIP4P/F water in the solid state (ice I_h and LDA) are in remarkably good agreement with experiments, this is not the case in supercooled liquid water. As shown in refs 40 and 41, the isothermal compressibility of water $\kappa_P(T) = 1/B(T)$ from PIMD simulations is considerably smaller than observed in experiments. It follows from refs 40 and 41 that the inclusion of NQE cannot reproduce the volume fluctuations (i.e., $\kappa_P(T)$) in liquid water. Yet, NQE are sufficient (and necessary) to reproduce such fluctuations in ice I_h and LDA.

Supplementary Material

Refer to Web version on PubMed Central for supplementary material.

ACKNOWLEDGMENTS

This work was supported by the SCORE Program of the National Institutes of Health under Award Number 1SC3GM139673 and the NSF CREST Center for Interface Design and Engineered Assembly of Low Dimensional Systems (IDEALS), NSF Grant Number HRD-1547380. This work was supported, in part, by a grant of computer time from the City University of New York High Performance Computing Center under NSF Grants CNS-0855217, CNS-0958379 and ALI-1126113.

DEDICATION

We dedicate this manuscript to Pablo G. Debenedetti on the occasion of his 70th birthday. P.G.D.'s pioneering research on liquids, glasses, and especially his contributions to our understanding of water have been a continuous source of inspiration for many of us.

REFERENCES

(1). Debenedetti PG Metastable Liquids: Concepts and Principles; Princeton University Press, 1996; Vol. 1.

(2). Franks F Water: a Matrix of Life; Royal Society of Chemistry, 2007.

(3). Levy Y; Onuchic JN Water mediation in protein folding and molecular recognition. Annu. Rev. Biophys. Biomol. Struct. 2006, 35, 389–415. [PubMed: 16689642]

(4). Rosu-Finsen A; Davies MB; Amon A; Wu H; Sella A; Michaelides A; Salzmann CG Medium-density amorphous ice. Science 2023, 379, 474–478. [PubMed: 36730416]

(5). Salzmann CG Advances in the experimental exploration of water's phase diagram. J. Chem. Phys. 2019, 150, 060901.

(6). Salzmann CG; Loveday JS; Rosu-Finsen A; Bull CL Structure and nature of ice xix. Nat. Commun. 2021, 12, 3162. [PubMed: 34039987]

(7). Loerting T; Winkel K; Seidl M; Bauer M; Mitterdorfer C; Handle PH; Salzmann CG; Mayer E; Finney JL; Bowron DT How many amorphous ices are there? Phys. Chem. Chem. Phys. 2011, 13, 8783–8794. [PubMed: 21431195]

(8). Kim KH; Amann-Winkel K; Giovambattista N; Spah A; Perakis F; Pathak H; Parada ML; Yang C; Mariedahl D; Eklund T; et al. Experimental observation of the liquid-liquid transition in bulk supercooled water under pressure. Sci. 2020, 370, 978–982.

(9). Amann-Winkel K; Kim KH; Giovambattista N; Ladd-Parada M; Spah A; Perakis F; Pathak H; Yang C; Eklund T; Lane TJ; et al. Liquid-liquid phase separation in supercooled water from ultrafast heating of low-density amorphous ice. Nat. Commun. 2023, 14, 442. [PubMed: 36707522]

(10). Mishima O; Calvert LD; Whalley E 'melting ice'i at 77 k and 10 kbar: A new method of making amorphous solids. Nature (London) 1984, 310, 393–395.

(11). Mishima O; Calvert LD; Whalley E An apparently first-order transition between two amorphous phases of ice induced by pressure. Nature (London) 1985, 314, 76–78.

(12). Mishima O Reversible first-order transition between two h2o amorphs at 0.2 gpa and 135 k. J. Chem. Phys. 1994, 100, 5910–5912.

(13). Angell CA Amorphous water. Annu. Rev. Phys. Chem. 2004, 55, 559–583. [PubMed: 15117262]

(14). Handle PH; Loerting T; Sciortino F Supercooled and glassy water: Metastable liquid (s), amorphous solid (s), and a no-man's land. Proc. Natl. Acad. Sci. U. S. A. 2017, 114, 13336–13344. [PubMed: 29133419]

(15). Encrenaz T Water in the solar system. Annu. Rev. Astron. Astrophys. 2008, 46, 57–87.

(16). Mayer E New method for vitrifying water and other liquids by rapid cooling of their aerosols. J. Appl. Phys. 1985, 58, 663–667.

(17). Venkatesh CG; Rice SA; Narten AH Amorphous solid water: An x-ray diffraction study. Science 1974, 186, 927–928. [PubMed: 17730916]

(18). Kim CU; Wierman JL; Gillilan R; Lima E; Gruner SM A high-pressure cryocooling method for protein crystals and biological samples with reduced background x-ray scatter. J. Appl. Crystallogr. 2013, 46, 234–241. [PubMed: 23396891]

(19). Pflugrath JW Practical macromolecular cryocrystallography. Acta Crystallogr. F:Struct. Biol 2015, 71, 622–642.

(20). Loerting T; Giovambattista N Amorphous ices: experiments and numerical simulations. J. Phys.: Condens. Matter 2006, 18, R919.

(21). Eltareb A; Lopez GE; Giovambattista N The role of high-density and low-density amorphous ice on biomolecules at cryogenic temperatures: a case study with polyalanine. Phys. Chem. Chem. Phys. 2021, 23, 19402–19414. [PubMed: 34494044]

(22). Giovambattista N; Eugene Stanley H; Sciortino F Phase diagram of amorphous solid water: Low-density, high-density, and very-high-density amorphous ices. Phys. Rev. E 2005, 72, 031510.

(23). Chiu J; Starr FW; Giovambattista N Pressure-induced transformations in computer simulations of glassy water. J. Chem. Phys. 2013, 139, 184504.

(24). Chiu J; Starr FW; Giovambattista N Heating-induced glass-glass and glass-liquid transformations in computer simulations of water. J. Chem. Phys. 2014, 140, 114504.

(25). Wong J; Jahn DA; Giovambattista N Pressure-induced transformations in glassy water: A computer simulation study using the tip4p/2005 model. J. Chem. Phys. 2015, 143, 074501.

(26). Engstler J; Giovambattista N Heating-and pressure-induced transformations in amorphous and hexagonal ice: A computer simulation study using the tip4p/2005 model. J. Chem. Phys. 2017, 147, 074505.

(27). Giovambattista N; Loerting T; Lukanov BR; Starr FW Interplay of the glass transition and the liquid-liquid phase transition in water. Sci. Rep. 2012, 2, 1–8.

(28). Giovambattista N; Sciortino F; Starr FW; Poole PH Potential energy landscape of the apparent first-order phase transition between low-density and high-density amorphous ice. J. Chem. Phys. 2016, 145, 224501.

(29). Ceriotti M; Fang W; Kusalik PG; McKenzie RH; Michaelides A; Morales MA; Markland TE Nuclear quantum effects in water and aqueous systems: Experiment, theory, and current challenges. Chem. Rev. 2016, 116, 7529–7550. [PubMed: 27049513]

(30). Gainaru C; Agapov AL; Fuentes-Landete V; Amann-Winkel K; Nelson H; Köster KW; Kolesnikov AI; Novikov VN; Richert R; Böhmer R; et al. Anomalously large isotope effect in the glass transition of water. Proc. Natl. Acad. Sci. U. S. A. 2014, 111, 17402–17407. [PubMed: 25422420]

(31). Liu Y; Sun G; Eltareb A; Lopez GE; Giovambattista N; Xu L Nuclear quantum effects on the thermodynamic response functions of a polymorphic waterlike monatomic liquid. Phys. Rev. Res. 2020, 2, 013153.

(32). Eltareb A; Lopez GE; Giovambattista N Nuclear quantum effects on the dynamics and glass behavior of a monatomic liquid with two liquid states. J. Chem. Phys. 2022, 156, 204502.

(33). Nguyen B; Lopez GE; Giovambattista N Nuclear quantum effects on the liquid−liquid phase transition of a water-like monatomic liquid. Phys. Chem. Chem. Phys. 2018, 20, 8210−8217. [PubMed: 29528051]

(34). Habershon S; Markland TE; Manolopoulos DE Competing quantum effects in the dynamics of a flexible water model. J. Chem. Phys. 2009, 131, 024501. [PubMed: 19603998]

(35). Röttger K; Endriss A; Ihringer J; Doyle S; Kuhs WF Lattice constants and thermal expansion of h2o and d2o ice ih between 10 and 265 k. Acta Crystallogr. B: Struct. Sci. Cryst. Eng. Mater. 1994, 50, 644–648.

(36). Buckingham DTW; Neumeier JJ; Masunaga SH; Yu Y-K Thermal expansion of single-crystal h 2 o and d 2 o ice ih. Phys. Rev. Lett. 2018, 121, 185505.

(37). Pamuk B; Soler JM; Ramirez R; Herrero CP; Stephens PW; Allen PB; Fernandez-Serra M-V Anomalous nuclear quantum effects in ice. Phys. Rev. Lett. 2012, 108, 193003.

(38). Herrero CP; Ramírez R Isotope effects in ice ih: A path-integral simulation. J. Chem. Phys. 2011, 134, 094510.

(39). Tanaka H Hydrogen bonds between water molecules: thermal expansivity of ice and water. J. Mol. Liq. 2001, 90, 323–332.

(40). Eltareb A; Lopez GE; Giovambattista N Nuclear quantum effects on the thermodynamic, structural, and dynamical properties of water. Phys. Chem. Chem. Phys. 2021, 23, 6914–6928. [PubMed: 33729222]

(41). Eltareb A; Lopez GE; Giovambattista N Evidence of a liquid-liquid phase transition in h_2o and d_2o from path-integral molecular dynamics simulations. Sci. Rep. 2022, 12, 1–14. [PubMed: 34992227]

(42). Ramírez R; Herrero CP Kinetic energy of protons in ice ih and water: A path integral study. Phys. Rev. B 2011, 84, 064130.

(43). Abascal JLF; Vega C A general purpose model for the condensed phases of water: Tip4p/2005. J. Chem. Phys. 2005, 123, 234505.

(44). Ramírez R; Neuerburg N; Fernandez-Serra M-V; Herrero CP Quasi-harmonic approximation of thermodynamic properties of ice ih, ii, and iii. J. Chem. Phys. 2012, 137, 044502.

(45). Eastman P; Friedrichs MS; Chodera JD; Radmer RJ; Bruns CM; Ku JP; Beauchamp KA; Lane TJ; Wang L-P; Shukla D; et al. Openmm 4: a reusable, extensible, hardware independent library for high performance molecular simulation. J. Chem. Theory Comput. 2013, 9, 461–469. [PubMed: 23316124]

(46). Ceriotti M; Parrinello M; Markland TE; Manolopoulos DE Efficient stochastic thermostatting of path integral molecular dynamics. J. Chem. Phys. 2010, 133, 124104.

(47). Tironi IG; Sperb R; Smith PE; van Gunsteren WF A generalized reaction field method for molecular dynamics simulations. J. Chem. Phys. 1995, 102, 5451–5459.

(48). Kohl I; Bachmann L; Hallbrucker A; Mayer E; Loerting T Liquid-like relaxation in hyperquenched water at ≤ 140 k. Phys. Chem. Chem. Phys. 2005, 7, 3210–3220. [PubMed: 16240034]

(49). Giovambattista N; Poole PH Liquid−liquid phase transition in simulations of ultrafast heating and decompression of amorphous ice. J. Non-Crys 2021, 11, 100067.

(50). Handle PH; Sciortino F; Giovambattista N Glass polymorphism in tip4p/2005 water: A description based on the potential energy landscape formalism. J. Chem. Phys. 2019, 150, 244506.

(51). Loerting T; Schustereder W; Winkel K; Salzmann CG; Kohl I; Mayer E Amorphous ice: Stepwise formation of very-high-density amorphous ice from low-density amorphous ice at 125 k. Phys. Rev. Lett. 2006, 96, 025702.

(52). $\alpha_P(T)$ is obtained by using eq 1 with the data included from Figure 1. Specifically, we extract the volumes of LDA and ice Ih from Figure 1a,b for T < 200 K and then fit these values using a polynomial of the form $V(T) = c_0 + c_2V^2 + c_3V^3$. The use of this polynomial is appealing because it agrees with the experimental values of $\alpha_P(T)$ at T ≥ 50 K (Figure 2), and it satisfies the third law of thermodynamics (i.e., $\lim_{T\to 0}\alpha_P(T) = 0$).

(53). Debenedetti P G Supercooled and glassy water. J. Phys.: Condens. Matter 2003, 15, R1669.

(54). Allen MP; Tildesley DJ Computer Simulation of Liquids; Oxford University Press, 2017.

(55). Neumeier JJ Elastic constants, bulk modulus, and compressibility of h2o ice i h for the temperature range 50 k−273 k. J. Phys. Chem. Ref. Data 2018, 47, 033101.

(56). Narten AH; Venkatesh C-G; Rice SA Diffraction pattern and structure of amorphous solid water at 10 and 77 k. J. Chem. Phys. 1976, 64, 1106–1121.

(57). Finney JL; Hallbrucker A; Kohl I; Soper AK; Bowron DT Structures of high and low density amorphous ice by neutron diffraction. Phys. Rev. Lett. 2002, 88, 225503.

(58). Errington JR; Debenedetti PG Relationship between structural order and the anomalies of liquid water. Nature (London) 2001, 409, 318–321. [PubMed: 11201735]

(59). Russo J; Tanaka H Understanding water's anomalies with locally favoured structures. Nat. Commun. 2014, 5, 1–11.

(60). Luzar A; Chandler D Effect of environment on hydrogen bond dynamics in liquid water. Phys. Rev. Lett. 1996, 76, 928. [PubMed: 10061587]

(61). Strässle Th; Saitta AM; Klotz S; Braden M Phonon dispersion of ice under pressure. Phys. Rev. Lett. 2004, 93, 225901.

(62). Karina A; Eklund T; Tonauer CM; Li H; Loerting T; Amann-Winkel K Infrared spectroscopy on equilibrated high-density amorphous ice. J. Phys. Chem. Lett. 2022, 13, 7965–7971. [PubMed: 35981100]

(63). Tuckerman M Statistical Mechanics: Theory and Molecular Simulation; Oxford University Press, 2010.

(64). The PIMD simulations for water in the vapor phase are performed for a system composed of N = 512 water molecules in a cubic box of V = 100 nm^3. The system is first equilibrated for 2 ns at constant volume at T = 400 K. After this equilibration, the system was then simulated at the same temperatures as was performed for ice I_h (see Simulation Method).

(65). Bachler J; Giebelmann J; Amann-Winkel K; Loerting T Pressure-annealed high-density amorphous ice made from vitrified water droplets: A systematic calorimetry study on water's second glass transition. J. Chem. Phys. 2022, 157, 064502.

(66). Mollica EM; Russo J; Stanley HE; Sciortino F Decompression dynamics of high density amorphous ice above and below the liquid-liquid critical point. J. Non-Crys. 2022, 13, 100081.

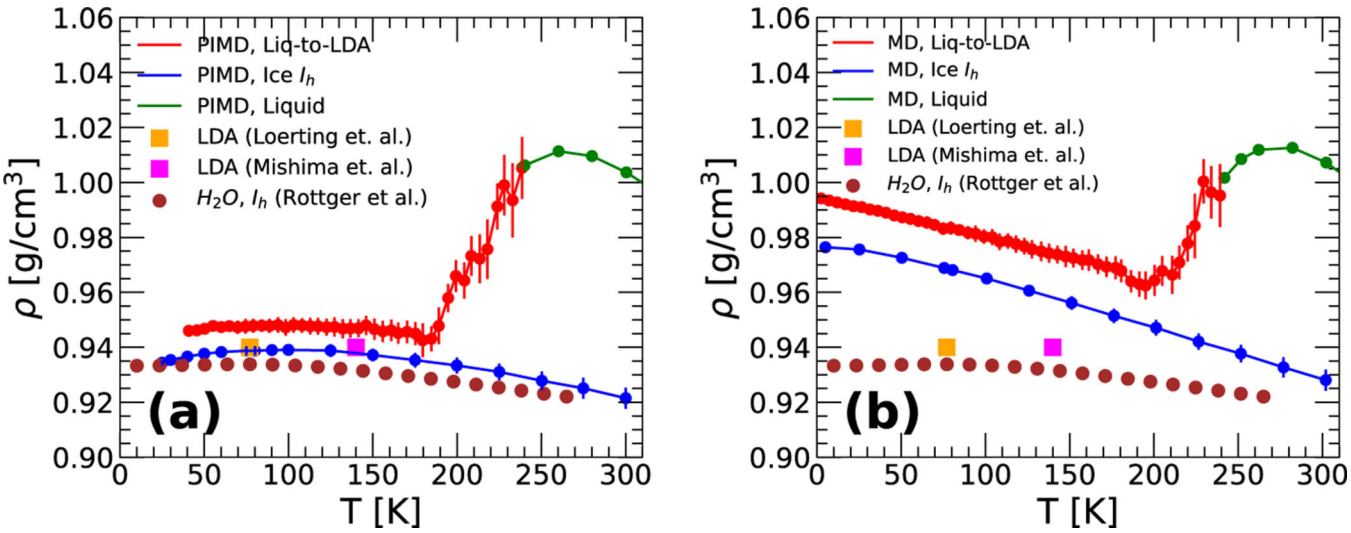

Figure 1.

Density $\rho(T)$ of H_2O at $P = 0.1$ MPa from (a) PIMD and (b) classical MD simulations using the q-TIP4P/F water model. Green circles are the densities of water in the equilibrium liquid state; red circles are the densities upon cooling liquid water from $T = 240$ K into the glass (LDA) state using a cooling rate of $q_T = 10$ K/ns. The magenta and orange squares are the experimental densities of LDA from refs 12 and 51. The blue circles are the densities of q-TIP4P/F water in the ice I_h state; the brown circles are the experimental densities of ice I_h reported in ref 35. While the densities of LDA and ice I_h are remarkably well reproduced by the PIMD simulations in (a), classical MD simulations overestimate considerably the corresponding densities. PIMD simulations (which include NQE) are consistent with the presence of a very weak density maximum in LDA and ice I_h. A very weak density maximum is also present in the experimental data of ice I_h (brown circles).[35]

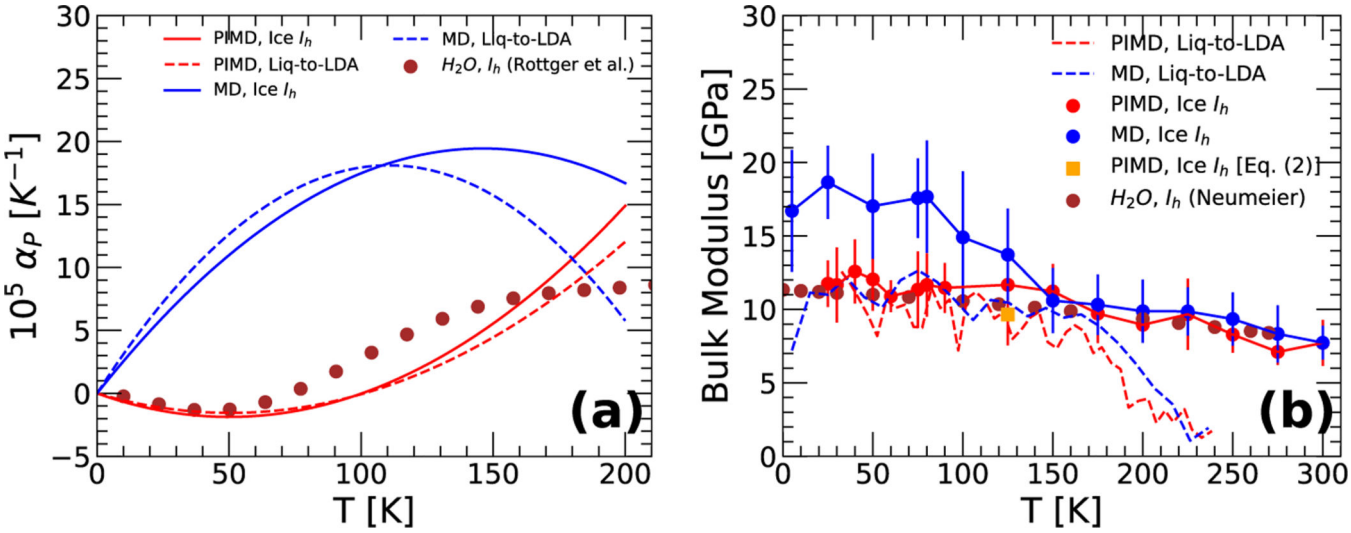

Figure 2.

(a) Thermal expansion coefficient $\alpha_P(T)$ and (b) bulk modulus $B(T)$ of ice I_h and during the liquid-to-LDA transformation at $P = 0.1$ MPa. Results are from PIMD (red lines) and classical MD simulations (blue lines). Dashed-lines are the results for H_2O during the isobaric cooling process from $T = 240$ K (liquid) into the LDA state ($q_T = 10$ K/ns). The solid lines correspond to H_2O in the equilibrium ice I_h state. For comparison, also included are the experimental values of $\alpha_P(T)$ and $B(T)$ for H_2O ice I_h (brown circles) from refs 35 and 55. Only the PIMD simulations (which include NQE) are able to reproduce approximately the behavior of $\alpha_P(T)$ and $B(T)$ for ice I_h. $B(T)$ is calculated using eq 3; the orange square in (b) corresponds to the value of $B(T)$ at $T = 125$ K obtained using eq 2.

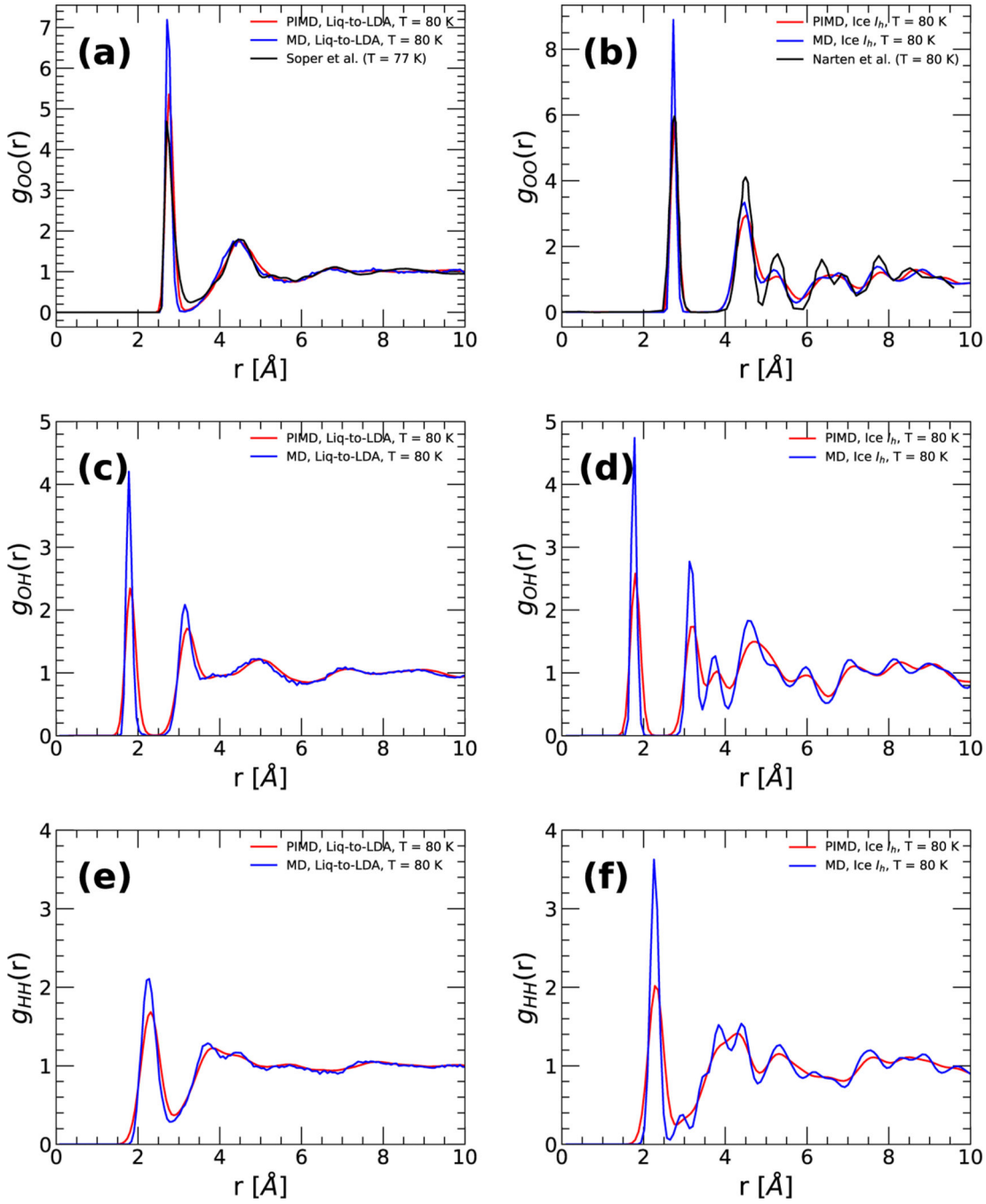

Figure 3.

(a), (c), and (e) are the oxygen−oxygen, oxygen−hydrogen, and hydrogen−hydrogen RDF of H_2O for LDA. (b), (d), and (f) are the OO, OH, and HH RDF of H_2O for ice I_h at $T = 80$ K and $P = 0.1$ MPa. Red and blue lines are the RDF obtained from PIMD and MD simulations, respectively, using the q-TIP4P/F model for water; black lines in (a) and (b) are the experimental OO RDF from ref 56 (ice I_h) and ref 57 (LDA). The inclusion of NQE reduces the maxima in the OO, OH, and HH RDF, leading to a less structured LDA and ice I_h.

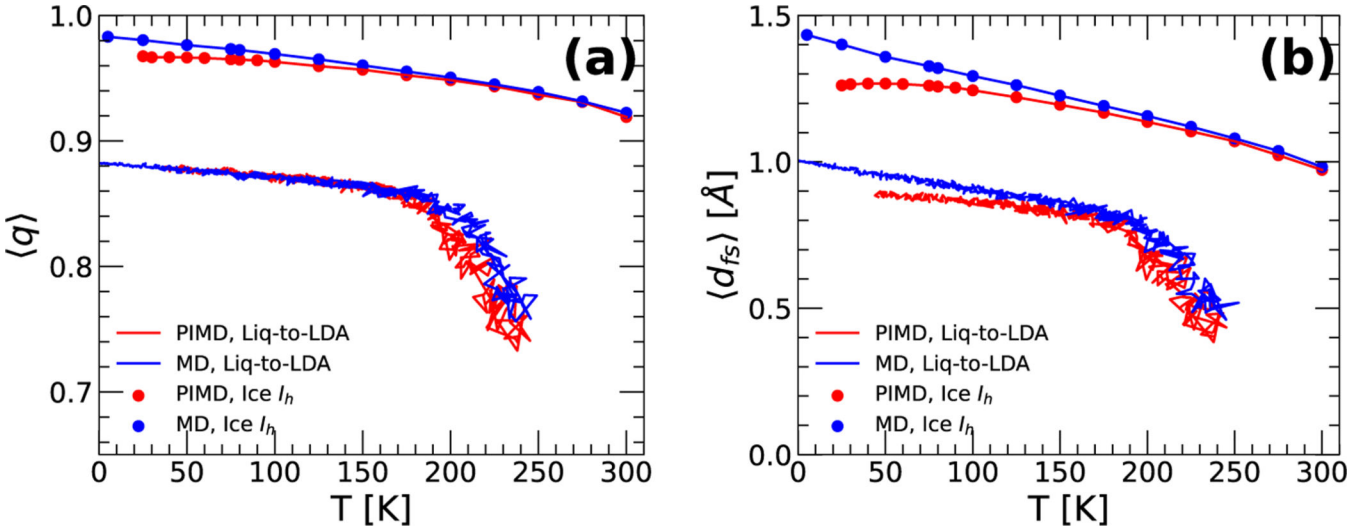

Figure 4.

(a) Tetrahedral order parameter $\langle q(T)\rangle$, and (b) $\langle d_{fs}(T)\rangle$ order parameter, for H_2O at $P = 0.1$ MPa. Circles are the order parameters for ice I_h; lines are the order parameters upon cooling the equilibrium liquid from $T = 240$ K into the glass state (LDA) using a cooling rate of $q_T = 10$ K/ns. Red and blue colors are results from PIMD and MD simulations using the q-TIP4P/F model for water. The similar values of $\langle q(T)\rangle$ and $\langle d_{fs}\rangle$ in the MD and PIMD simulations suggest that the inclusion of NQE on the local order of water are rather weak.

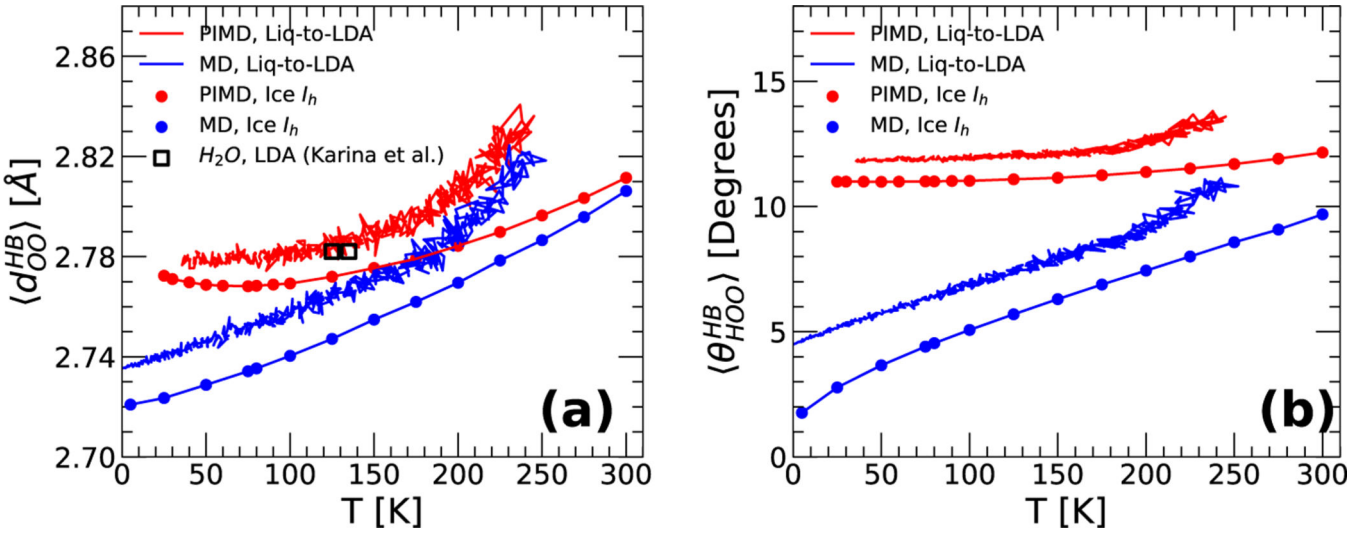

Figure 5.

(a) Average distance between two oxygen atoms forming a hydrogen-bond, $\langle d_{OO}^{HB}(T) \rangle$, as a function of temperature and at $P = 0.1$ MPa. Circles are the $\langle d_{OO}^{HB}(T) \rangle$ for ice I_h; lines are the $\langle d_{OO}^{HB}(T) \rangle$ for water upon cooling the equilibrium liquid from $T = 240$ K into the glass state (LDA) using a cooling rate $q_T = 10$ K/ns. Red and blue colors are results from PIMD and classical MD simulations using the q-TIP4P/F model for water. Experimental values of $d_{OOO}^{HB}(T)$ in LDA from IR spectroscopy experiments are indicated by black squares (from ref 62).(b) Average HOO angle formed between two hydrogen-bonded watermolecules, $\langle \theta_{HOO}^{HB}(T) \rangle$, as a function of temperature at $P = 0.1$ MPa. Same symbols and colors as in (a) are used. The inclusion of NQE leads to slightly longer hydrogen-bond lengths (larger $\langle d_{OO}^{HB}(T) \rangle$) and less linear hydrogen-bonds (larger $\langle \theta_{HOO}^{HB}(T) \rangle$) than predicted by classical MD simulations.

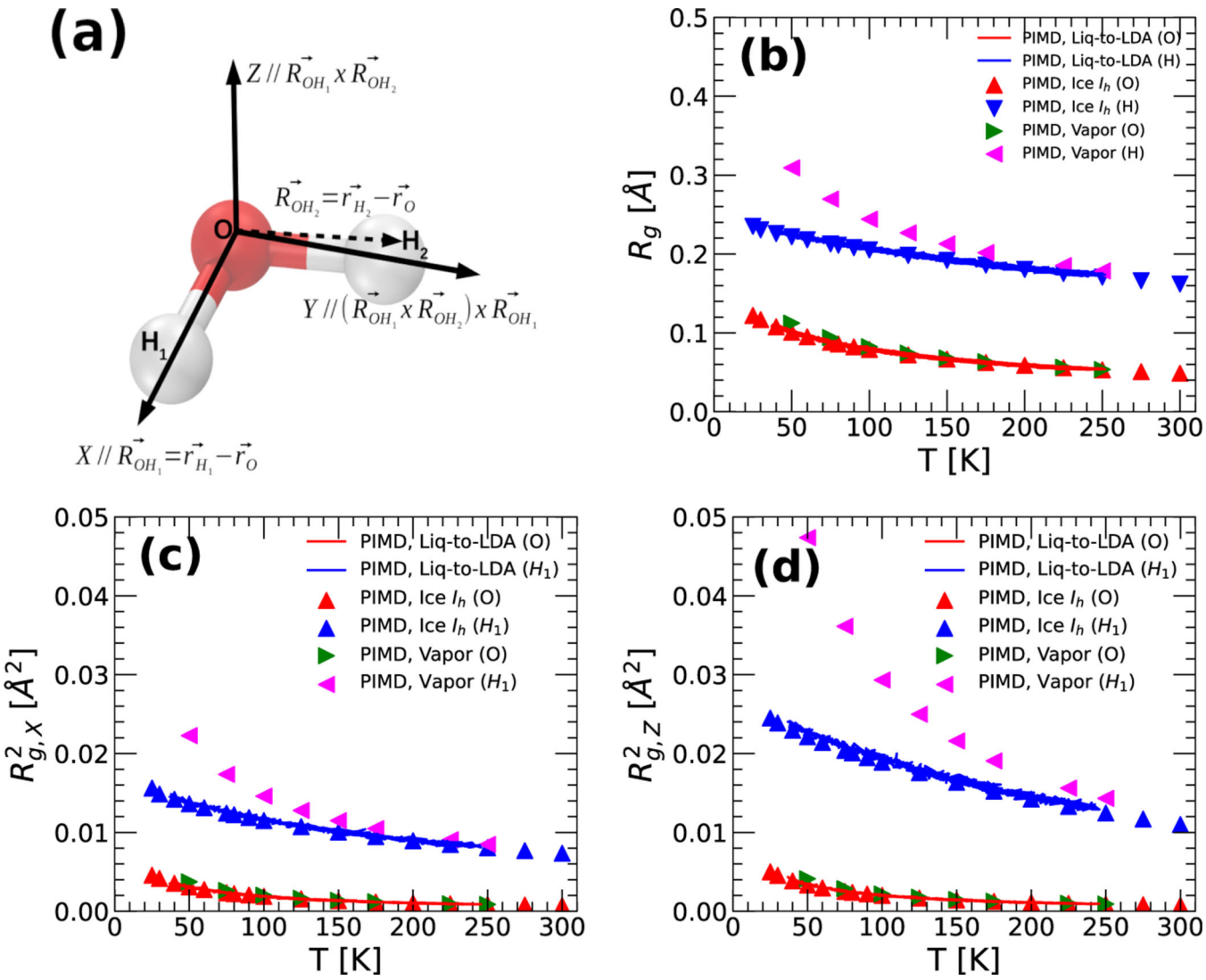

Figure 6.

Delocalization of the O and H atoms in ice I_h and during the isobaric cooling of liquid water into LDA ($P = 0.1$ MPa). Results are from classical MD and PIMD simulations using the q-TIP4P/F water model. (a) Schematic diagram showing a water molecule and the corresponding reference frame used in (b)−(d). For a given water molecule, the reference frame origin is located on the O centroid. $\vec{R}_{OH_j}$ is the vector pointing from the O centroid to the centroid of $H_j (j = 1, 2)$. The *x*-, *y*-, and *z*-axis are defined as indicated in the figure. (b) Radius of gyration $R_g(T)$ of the ring-polymers associated with the O and H atoms as a function of temperature. Red and blue lines are the $R_g(T)$ for the H and O during the cooling process from $T = 240$ K (liquid state) to $T = 25$ K (LDA) using a cooling rate $q_T = 10$ K/ns; the red and blue triangles are the $R_g(T)$ of the O and H in ice I_h. The delocalization of the O and H atom is identical for water in the liquid/LDA and ice I_h states, probably due to the similar local structure. O and H atoms are more delocalized in the low-density vapor state (magenta triangles), particularly at low temperatures. (c, d) Delocalization of

the ring-polymers associated with the O and H_1 atoms along the x- and z-axis, respectively (similar results are obtained along the y- and z-axis). $R^2_{g,x}$ and $R^2_{g,z}$ are the x- and z-radius of gyration (see text). Same symbols as in (b) are used. For the O atoms, $R^2_{g,x} \approx R^2_{g,z}$, meaning that the O delocalization is isotropic. Instead, for the H_1 atoms, $R^2_{g,z} > R^2_{g,x}$, i.e., the H atoms are more delocalized along the directions perpendicular to the corresponding OH covalent bonds than along the OH bond direction; see Figure 7.

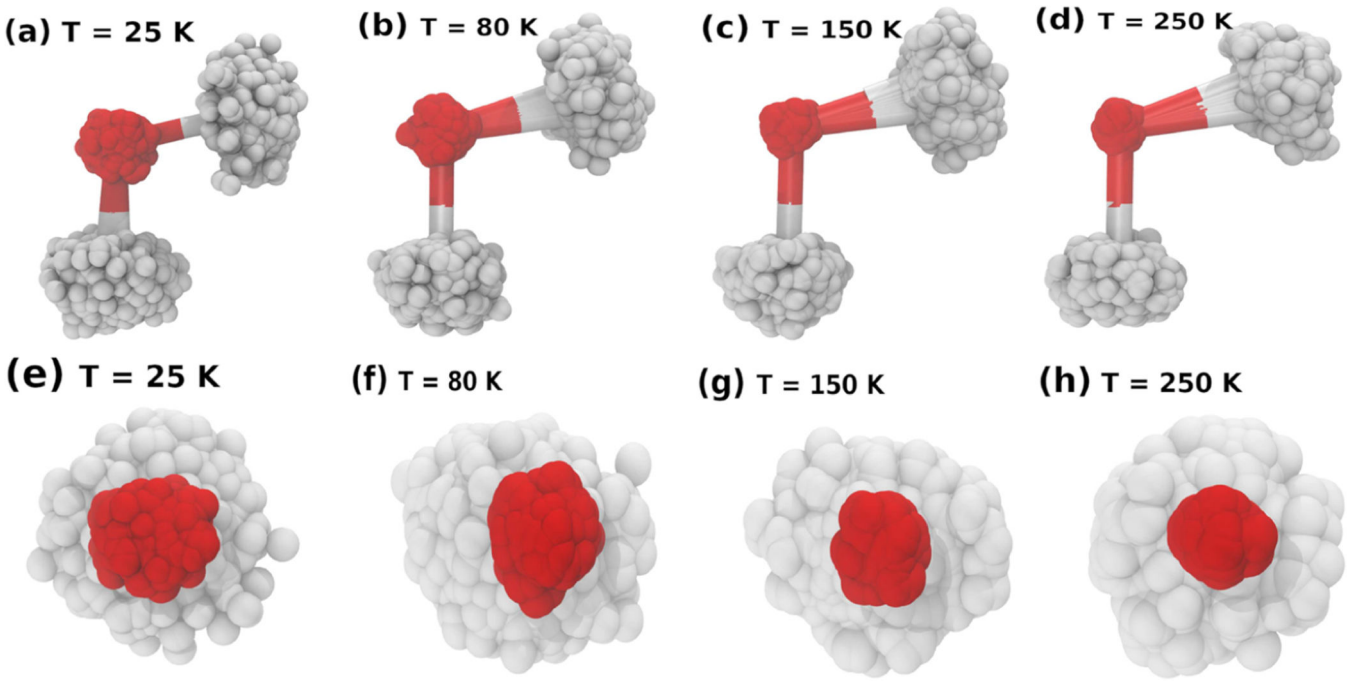

Figure 7.

Snapshots of an H_2O molecule obtained from PIMD simulations of ice I_h at $P = 0.1$ MPa and $T = 25$, 80, 150, and 250 K (similar results hold for H_2O in the LDA state, see Figure S3 of the SI). In (a)−(d), the water molecule is laying on the x-y plane defined in Figure 6a. The O and H ring-polymer beads are shown by small red and white spheres, respectively; all ring-polymers are composed of $n_b = 128$. (e−h) Snapshot of the water molecule shown in (a)−(d), showing the O atom and only one of the H atoms; the view is along the corresponding OH covalent bond. The delocalization of the O atom is rather isotropic, i.e., the red cloud of ring-polymer beads is rather spherical. The delocalization of the H atoms is anisotropic; the white cloud of ring-polymer beads are spread preferentially along the directions perpendicular to the OH covalent bond direction (than along the OH covalent bond direction). Similar results are also obtained for D_2O in ice I_h and LDA, see Figures S10 and S12 of the SI.

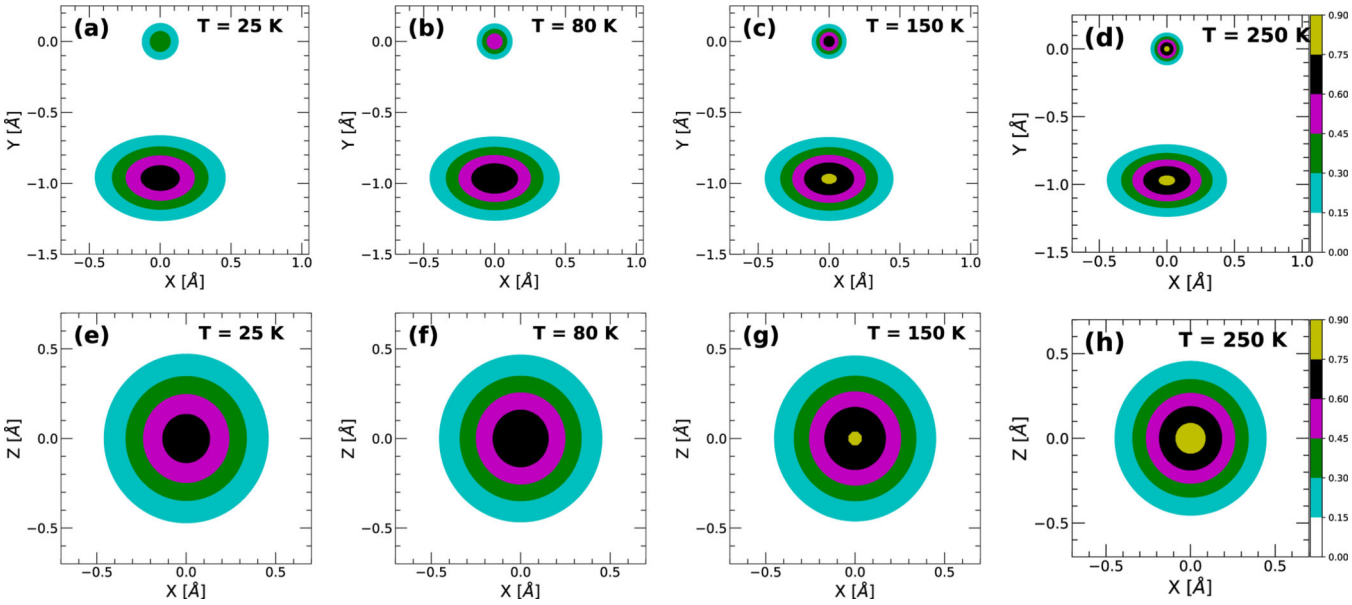

Figure 8.

Contour maps for the probability distribution to find a ring-polymer bead. $P = 0.1$ MPa and $T = 25$, 80, 150, and 250 K. (a)−(d) Ring-polymer bead probability distribution associated with the O (top) and H (bottom) atoms in ice I_h (similar results hold for the case of LDA, see Figure S4 of the SI); see also Figure 6a–d. Contour maps are projected on the *x*-*y* plane shown in Figure 6a; see also Figure 7a–d. (e)−(h) are the contour maps for the probability distribution associated with the H atoms projected on the plane perpendicular to the corresponding OH covalent bond (i.e., viewed along the OH covalent bond; see also Figure 7e–h). All probability distributions are averaged over time and over all atoms in the system. Similar results are obtained for D_2O in the ice I_h and LDA states; see Figures S11 and S13 in the SI.